DOI: 10.1002/adma.200800485

Elastic Properties and Buckling of Silicon Nanowires**

By *Cheng-Lun Hsin, Wenjie Mai, Yudong Gu, Yifan Gao, Chi-Te Huang, Yuzi Liu, Lih-Juann Chen,** and *Zhong-Lin Wang**

Silicon is the most important material for the electronics industry. Its unique electronic, optoelectronic, thermal, and mechanical properties have made Si an ideal choice for integrated circuits, memory devices, solar cells, and micro-electromechanical systems (MEMS).[1–4] Considering one-dimensional (1D) nanomaterials, carbon nanotubes, silicon nanowires, and ZnO nanowires/nanobelts are the three primary structures of choice, because of their largely improved, different, and/or unique properties at the nanometer scale.[5–8] As the sizes of MEMS approach nanoelectromechanical systems (NEMS),[9] exploration of the changes of mechanical properties on the nanometer scale is vitally important.[10–15] Silicon nanowires (NWs) are the key building blocks of future electronics.[16] Several approaches have been developed to study the mechanical behavior of Si nanowires.[17–21] The existing literature reports progress in observing the phenomenon of plasticity and in measuring the elastic modulus of single NWs or NW arrays. In this Communication, we report using a manipulation probe and an atomic force microscope (AFM) tip in scanning electron microscopy (SEM) to investigate the mechanical behavior of a single SiNW under buckling and bending conditions. Some of the mechanical properties of SiNWs have been quantified. Our study has demonstrated the tough and robust behavior of SiNWs.

The SiNWs used for our experiments were fabricated by chemical vapor deposition by the vapor–liquid–solid (VLS) growth process.[22] Figure 1 shows a transmission electron microscopy (TEM) image of an as-grown SiNW, revealing its core/shell structure. The diameters of the NWs are 40–90 nm. The thickness of the outer native oxide layer is about 5 nm. The inset shows a diffraction pattern, revealing the single-crystalline structure of the NWs.

[*] Prof. Z.-L. Wang, C.-L. Hsin, W. J. Mai, Y. D. Gu, Y. F. Gao, Dr. Y. Z. Liu
School of Materials Science and Engineering
Georgia Institute of Technology
Atlanta, GA 30332-0245 (USA)
E-mail: zhong.wang@mse.gatech.edu
Prof. L.-J. Chen, C.-L. Hsin, C.-T. Huang
Department of Materials Science and Engineering
National Tsing Hua University
Hsinchu, Taiwan 30043 (Taiwan)
E-mail: ljchen@mx.nthu.edu.tw

[**] C. L. Hsin and W. J. Mai contributed equally to this work. This work was supported by DOE BES (DE-FG02-07ER46394), NSF (DMS 0706436), and the National Science Council of the Republic of China (Taiwan) under grant NSC 96-2120-M-007-006.

The SiNW was manipulated using a tungsten probe, and the AFM cantilever was used to measure the force–displacement response of a single SiNW. Figures 2a and b schematically illustrate the principle of the mechanical manipulation setup. First, as shown in Figure 2a, the SiNW was attached to the probe. Then the SiNW was bent by pushing the probe against the AFM cantilever. The AFM cantilever was deflected, as shown in Figure 2b, from which the displacement and the applied force could be quantified, provided the mechanical behavior of the cantilever is well characterized. The displacement was characterized by the distance between the two ends of the NW.

Figure 3 shows a series of images and the corresponding bending curves measured from a single SiNW when it was buckled by the probe. It is important to make sure that the NW is oriented perpendicular to the direction of the electron beam to ensure that there is no ''hidden'' displacement along the electron beam direction. This is important in order to measure the displacement precisely. In Figures 3a–f the SiNW is shown being pushed against the AFM cantilever, and the deflection of the cantilever is clearly presented in the images with reference to a stationary feature at the top of the images, which is not connected to the cantilever and is out of focus in the images due to the difference in depth. With this stationary feature as a reference point, the NW deflection as well as the bending force can be quantified. The NW was affixed at its two ends to the tip and the cantilever. We used the straight distance between the two ends of the NW (L) to characterize its buckling effect. Figure 3g shows a curve that presents the applied force, as measured from the deflection of the cantilever, versus the absolute value of the difference of the chord, i.e., $|L - L_0|$. The curve presented the standard buckling behavior of a slender column under the action of an axial load.

Figure 3h shows the calculated curve of the stress and strain based on Figure 3g. Under the approximation that the strain was homogeneous and the NW would become semicircular at the maximum deformation, we can solve the equations $R\alpha = L_0$ and $[R \sin(\alpha/2)] = L/2$, as depicted in the inset of Figure 3h. The stress was expressed as a function of the applied force F and the cross-sectional area of the NW A: stress $= F/A$. The strain was expressed as a function of diameter of the NW d and the radius of curvature R: strain $= d/2R$. At the maximum elastic point in this experiment, the strain of the NW was ca. 1.5%, much higher than the 0.2% for most typical metallic materials.[23]

Figure 4 shows the experimental and calculated data of the strain versus $|L - L_0|$ during the buckling. In the calculation, the relationship between the buckled chord length L and the

ADVANCED MATERIALS

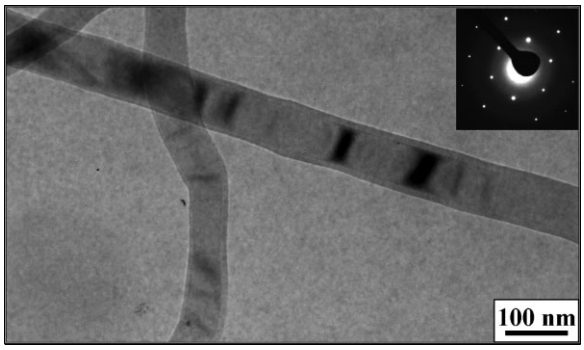

Figure 1. TEM image of the SiNWs with 5–10 nm native oxide layer. Inset: Selected area electron diffraction pattern.

strain ε is calculated with a thin rod model.[24] We suppose that the buckling force applied by the AFM cantilever is parallel to the original unbuckled nanowire. The shape of the bent nanowire is described by a schematic model (inset in Fig. 4), which is given in the following form:

$$x = \sqrt{2}\lambda \times \left[\sqrt{1-\cos\theta_0} - \sqrt{\cos\theta - \cos\theta_0}\right]$$
$$y = \frac{1}{\sqrt{2}}\lambda \int_0^{\theta} \frac{\cos\theta}{\sqrt{\cos\theta - \cos\theta_0}} \quad (1)$$

where θ is the local orientation of the tangent to the nanowire. λ is a characteristic length, defined as $\lambda = (EI_0/f)^{1/2}$, where E is Young's modulus, I_0 is the moment of inertia of the cross section, and f is the magnitude of the buckling force. $\theta_0 = \theta(L_0)$ is the local orientation at the top of the nanowire, where L_0 is the chord length of the unbuckled wire, that is, the length of the nanowire. The maximum strain that occurs at the surface of the nanowire is

$$\varepsilon_{\max} = r\frac{d\theta}{dl} = r\frac{1}{dl/d\theta} \quad (2)$$

where r is the radius of the nanowire and

$$l = l(\theta) = \sqrt{1/2}\lambda \int_0^{\theta} \frac{d\theta}{\sqrt{\cos\theta - \cos\theta_0}} \quad (3)$$

is the arc length from the bottom of the wire to the point (x,y) in discussion.[24]

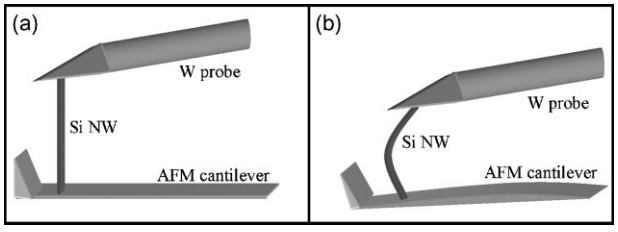

Figure 2. Schematic diagram illustrating the experimental setup before (a) and after (b) the manipulation.

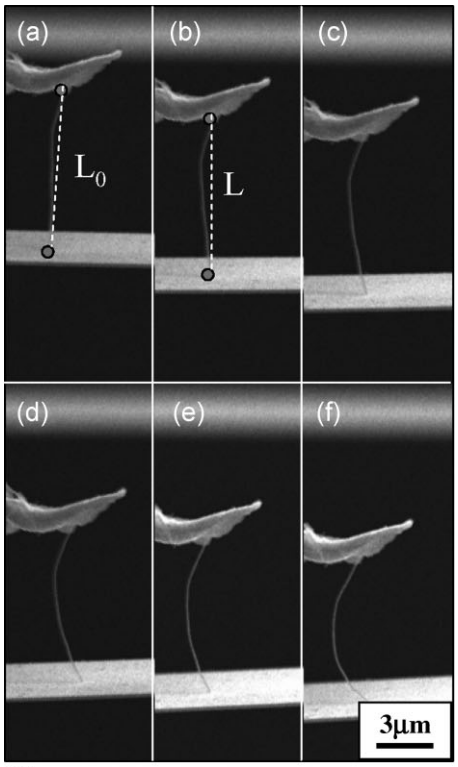

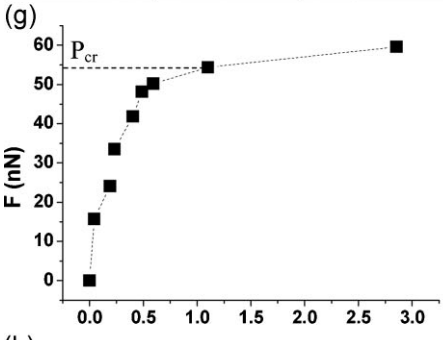

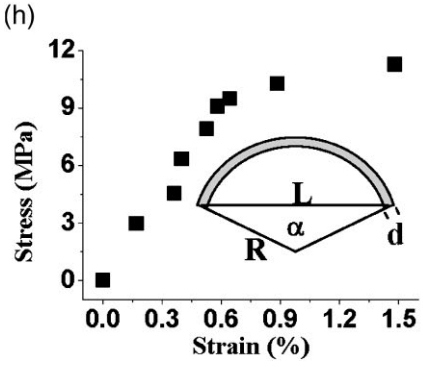

Figure 3. a–f) A series of snapshot SEM images showing the continuous buckling of the SiNW. g) Corresponding curve of the applied force F vs. change in chord length $|L - L_0|$ when the NW was buckled. h) Calculated stress–strain curve of the buckling of the NW. Inset: Schematic diagram of the deformation approximation.

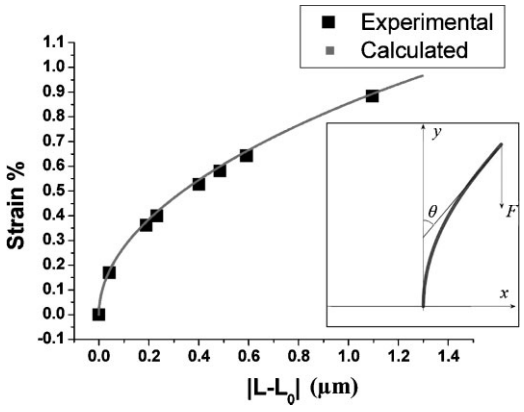

Figure 4. A comparison of the experimental results and simulated curve of strain vs. change in chord length $|L - L_0|$. Inset: Schematic model of the nanowire under buckling. The calculation was carried out for the middle point of the chord: $l = L_0/2$.

The maximum strain is a function of l. We have calculated ε_{max} for the position $l = L_0/2$, that is, at the middle of the wire. Then the strain versus chord length plot is as given in Figure 4. The calculated curve matched the experimental data well, indicating that the assumption fits well for Figure 3h. The results demonstrate that the strain of the NW is larger than the conventional value for bulk materials.

The critical load P_{cr}, which is defined as the load higher than which a clearly non-linear and buckling deformation occurs, is marked in Fig. 3. After reaching the critical force, a slight increase of the force caused the NW to buckle. The NW returned to its original shape when the load was removed, showing the ultrahigh toughness of the NW. The force-deflection curves obtained in this measurement share a highly similar tendency with the curves for buckling effect, which is explained by Euler's formula. From Euler's formula,[25] which can be expressed as a function of the elastic modulus E, moment of inertia I_0, length of the NW L_0, and an effective factor K such that $P_{cr} = \pi^2 EI_0/(KL_0)^2$, the critical loads in our experiment are used to evaluate the elastic modulus of the NW (assuming the validity of Euler's formula). Because both ends of the NW were pinned, the effective factor K was equal to 1. Figure 5 shows the P_{cr} versus I_0/L^2 curve for a few NWs with different diameters and lengths. Euler's formula indicates that the slope of the curve is equal to $\pi^2 E$, giving the mean elastic modulus of the NWs $E = 175$ GPa, which is consistent with the

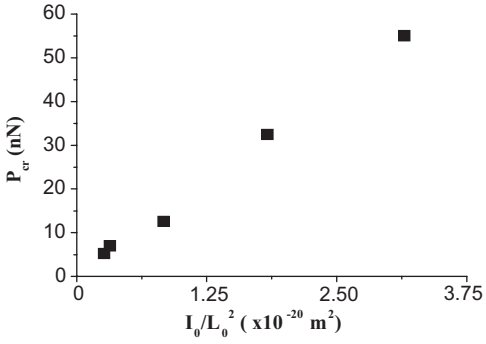

Figure 5. Plot of the critical load P_{cr} vs. I_0/L^2 for several NWs that have been manipulated.

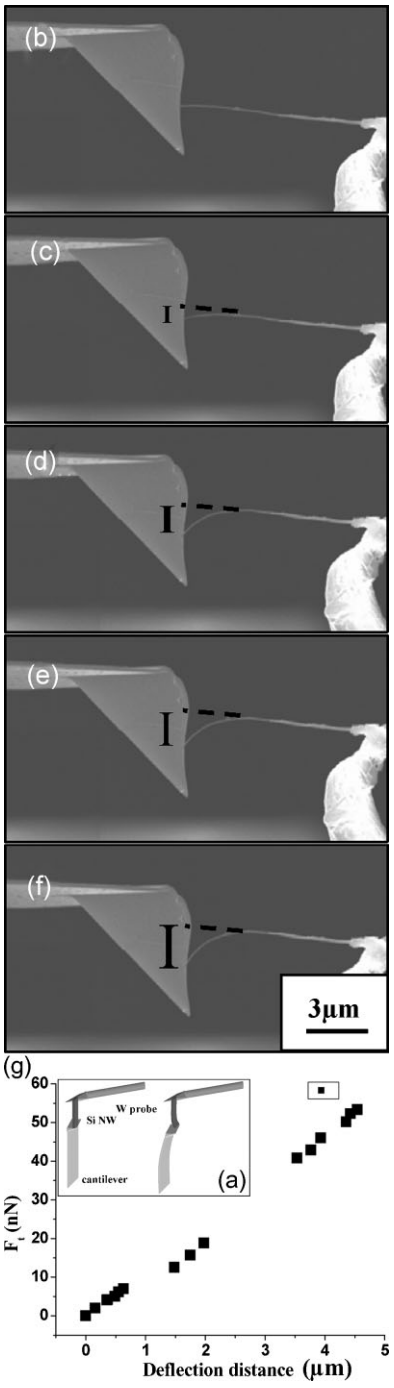

Figure 6. a) Schematic diagram illustrating the principle of bending and the setup. b–f) A series of snapshot SEM images showing the manipulation and deflection of a SiNW. g) Corresponding force–deflection distance curve of the NW.

ADVANCED MATERIALS

bulk value.[26] This result means that the elastic modulus of the NW is the same as the bulk value and is not changed by the reduction to a nanometer scale.

The elastic modulus of the NW can also be measured by applying the force along different directions, similar to the principle of AFM measurement.[27] Figure 6a is a schematic diagram of the manipulation process. First, a SiNW was attached to the probe and the head of the AFM. Then the SiNW was bent by moving the probe parallel to the AFM cantilever (vertically in Fig. 6a), which caused the AFM cantilever to bend because of a small horizontal force created by the NW. Once again, we used the stationary feature at the bottom of the images (Figs. 6b–f) as a reference to calculate the tangential force F_t along the vertical direction (Figs. 6b–f) and the bending of the NW in the vertical direction.

Figures 6b–f show snapshots of a SiNW when it was pushed against the head of the AFM cantilever; the deflection of the cantilever is shown in the image with reference to the static feature. The elastic modulus E can also be expressed as $E = kL_0^3/3I_0$ (where k is the spring constant). Figure 6g shows a curve that presents the tangential force, as measured from the deflection of the cantilever, versus the deflection distance. From the curve, the elastic modulus was determined to be ca. 200 GPa. In the regime of large deflection distances, the mechanical behavior of the NW is about the same as in the small-deflection linear part. This observation reveals that the linear regime of the NW is rather large. This could be helpful for the prediction of mechanical response and the design of the mechanical devices in NEMS.

For all of the SiNWs, the compressive load buckled the NW but did not fracture it even under extremely large deformation. The dramatic increase in flexibility is the result of the decreased thickness of the object.[19] For a slab of a material that has a thickness d, the elongation of the interatomic bond at the outer surface of the NW is $d\alpha/2$. If the critical bonding length before a bond breaks is s, under the condition of no generation of a dislocation, the maximum bending angle of the slab is $\alpha = 2s/d$. This means that the degree of bending is determined by the thickness of the object rather than its aspect ratio. For a NW of diameter ca. 20 nm, its bending angle is 1000 times of that of a silicon wafer of thickness 20 μm. At the maximum elastic point in this experiment, the strain of the NW was ca. 1.5%, much larger than the conventional value of 0.2%. In addition, a change in crystallinity for nanowires may also contribute to their much enhanced flexibility.

In summary, we have investigated the mechanical properties of single SiNWs using an in situ technique in a scanning electron microscope. The SiNW showed ultrahigh flexibility and strong toughness. The force–deflection distance curve in the large-displacement regime demonstrated that the mechanical behavior of the NW still follows Hooke's law. The experimental data and calculated results show that the NW can bear a large strain of 1.5%, much more than the bulk material. The elastic constant of the NW was determined to be 175–200 GPa. This study clearly demonstrates the flexibility and mechanical toughness of SiNWs.

Experimental

Synthesis of the SiNWs: SiNWs were synthesized by a vapor transport and condensation process using Au as a catalyst. The quartz tube inside the three-zone furnace was evacuated to a pressure below 10^{-5} Torr (1 Torr ≈ 133 Pa) using a diffusion pump. During the growth procedure, a constant flow of 60 sccm Ar and 15 sccm H_2 was introduced as the carrier gas and the pressure inside the quartz tube was kept constant at 1 Torr. The three zones were heated from room temperature to 1100, 900, and 700 °C, respectively, at the same time. The Si source in an alumina boat was placed upstream in the 1100 °C zone. Au-coated Si substrates were heated downstream in the middle of the 900 and 700 °C zones. After the samples had been kept at the desired temperature for 90 min, the furnace was cooled down to room temperature.

Morphology and Structure Characterization: The as-synthesized SiNWs were characterized by TEM (Hitachi 2000).

Sample Preparation: SiNWs were dispersed uniformly in ethanol solution. Immersing a tungsten probe in the solution for several seconds caused a SiNW to be attached to the tip, as could be checked with an optical microscope. The samples were annealed in a vacuum furnace at 300 °C at 50 sccm Ar flow under 10 Torr.

Mechanical Property Measurement: A tungsten probe with a SiNW was located on a manipulator, which could be remotely controlled in three dimensions. The length of the NW was estimated by rotating the NW in a LEO 1530 scanning electron microscope. The cross section was assumed to be round. The commercial AFM cantilever was made of Si_3N_4 with a spring constant of 0.006 N m^{-1} and loaded on a rotator that could be rotated through 360 °.

Received: February 19, 2008
Revised: April 16, 2008
Published online: September 3, 2008

[1] G. Stollwerck, S. Reber, C. Haßler, *Adv. Mater.* **2001**, *13*, 1820.
[2] T. M. Mayer, J. W. Elam, S. M. George, P. G. Kotula, R. S. Goeke, *Appl. Phys. Lett.* **2003**, *82*, 2883.
[3] Y. C. Lin, K. C. Lu, W. W. Wu, J. W. Bai, L. J. Chen, K. N. Tu, Y. Huang, *Nano Lett.* **2008**, *8*, 913.
[4] H. T. Chen, S. I. Hsieh, C. J. Lin, Y. C. King, *IEEE Electron Device Lett.* **2007**, *28*, 499.
[5] C. M. Lieber, Z. L. Wang, *MRS Bull.* **2007**, *32*, 99.
[6] Z. H. Chen, J. Appenzeller, Y. M. Lin, J. Sippel-Oakley, A. G. Rinzler, J. Y. Tang, S. J. Wind, P. M. Solomon, P. Avouris, *Science* **2006**, *311*, 1735.
[7] Y. Cui, C. M. Lieber, *Science* **2001**, *291*, 851.
[8] Z. W. Pan, Z. R. Dai, Z. L. Wang, *Science* **2001**, *291*, 1947.
[9] K. L. Ekinci, X. M. H. Huang, M. L. Roukes, *Appl. Phys. Lett.* **2004**, *84*, 4469.
[10] Y. F. Zhang, X. D. Han, K. Zheng, Z. Zhang, X. N. Zhang, J. Y. Fu, Y. Ji, Y. J. Hao, X. Y. Guo, Z. L. Wang, *Adv. Funct. Mater.* **2007**, *17*, 3435.
[11] R. R. He, P. D. Yang, *Nat. Nanotechnol.* **2006**, *1*, 42.
[12] M. F. Yu, O. Lourie, M. J. Dyer, K. Moloni, T. F. Kelly, R. S. Ruoff, *Science* **2000**, *287*, 637.
[13] P. X. Gao, W. J. Mai, Z. L. Wang, *Nano Lett.* **2006**, *6*, 2536.
[14] X. D. Bai, D. Golberg, Y. Bando, C. Y. Zhi, C. C. Tang, M. Mitome, K. Kurashima, *Nano Lett.* **2007**, *7*, 632.
[15] W. Z. Rong, W. Q. Ding, L. Madler, R. S. Ruoff, S. K. Friedlander, *Nano Lett.* **2006**, *6*, 2646.
[16] L. J. Chen, *J. Mater. Chem.* **2007**, *17*, 4639.
[17] X. D. Han, K. Zheng, Y. F. Zhang, X. N. Zhang, Z. Zhang, Z. L. Wang, *Adv. Mater.* **2007**, *19*, 2112.
[18] X. X. Li, T. Ono, Y. L. Wang, M. Esashi, *Appl. Phys. Lett.* **2003**, *83*, 3081.

[19] S. Hoffmann, I. Utke, B. Moser, J. Michler, S. H. Christiansen, V. Schmidt, S. Senz, P. Werner, U. Gösele, C. Ballif, *Nano Lett.* **2006**, *6*, 622.
[20] A. S. Paulo, N. Arellano, J. A. Plaza, R. He, C. Carraro, R. Maboudian, R. T. Howe, J. Bokor, P. D. Yang, *Nano Lett.* **2007**, *7*, 1100.
[21] A. Heidelberg, L. T. Ngo, B. Wu, M. A. Phillips, S. Sharma, T. I. Kamins, J. E. Sader, J. J. Boland, *Nano Lett.* **2006**, *6*, 1101.
[22] C. T. Huang, C. L. Hsin, K. W. Huang, C. Y. Lee, P. H. Yeh, U. S. Chen, L. J. Chen, *Appl. Phys. Lett.* **2007**, *91*, 093133.
[23] B. E. Schuster, Q. Wei, M. H. Ervin, S. O. Hruszkewycz, M. K. Miller, T. C. Hufnagel, K. T. Ramesh, *Scr. Mater.* **2007**, *57*, 517.
[24] L. D. Landau, E. M. Lifshitz, Theory of Elasticity, Course of Theoretical Physics, Vol. 5, Pergamon, Oxford **1959**.
[25] S. P. Timoshenko, J. M. Gere, *Theory of Elastic Stability*, McGraw-Hill, New York **1961**, *p.* 46.
[26] A. S. Paulo, J. Bokor, R. T. Howe, R. He, P. D. Yang, D. Gao, C. Carraro, M. Maboudian, *Appl. Phys. Lett.* **2005**, *87*, 053111.
[27] J. H. Song, X. D. Wang, E. Riedo, Z. L. Wang, *Nano Lett.* **2005**, *5*, 1954.

